Posted on 16 Nov 2022 — The copyright holder is the author/funder. All rights reserved. No reuse without permission. — https://doi.org/10.1002/essoar.10511958.1 — This a preprint and has not been peer reviewed. Data may be preliminary.

Identifying Abnormal Tank Emissions Using Ethane to Methane Signatures of Oil and Natural Gas Production in the Permian Basin

Caulton Dana R[1], Gurav Priya D[2], Robertson Anna M[2], Pozsonyi Kristen[2], Murphy Shane[2], and Lyon David R.[3]

[1]University of Wyoming
[2]University of Wyoming
[3]Environmental Defense Fund

November 16, 2022

Abstract

There has been increasing interest in quantifying methane emissions from a view towards mitigation. Accordingly, ground-based sampling of oil and gas production sites in the Permian Basin was carried out in January and October 2020. Ethane to methane ratios (EMRs) were quantified which may be used to distinguish emissions from particular sources, such as produced gas and oil tank flashing. The logarithmic mean EMR for 102 observations was 18 (±2)%, while source specific EMRs showed that sites where emissions were attributed to a tank produced much higher EMRs averaging 44%. Sites with other noticeable sources such as compressors, pneumatics, and separators had lower and less variable EMRs. Tanks displayed distinct behavior with EMRs between 10-21% producing CH_4 emissions >30x higher than tanks with EMRs >21%. This observation supports the hypothesis that high emission rate tank sources are often caused by separator malfunctions that leak produced gas through liquids storage tanks.

Identifying Abnormal Tank Emissions Using Ethane to Methane Signatures of Oil and Natural Gas Production in the Permian Basin

Dana R. Caulton[1], Priya D. Gurav[1], Anna. M. Robertson[1], Kristen Pozsonyi[1], Shane M. Murphy[1], David R. Lyon[2]

[1] Department of Atmospheric Science, University of Wyoming, Laramie, WY, USA.

[2] Environmental Defense Fund, Austin, TX, USA.

Corresponding author: Dana R. Caulton (dcaulton@uwyo.edu)

Key Points:

- Oil and gas production sites in the Permian Basin had a logarithmic mean ethane to methane ratio of 18%.
- Source specific ethane to methane ratios showed that on average tanks on production sites had higher ratios at 44%.
- Tanks with high ethane to methane ratios had statistically lower methane emissions than tanks with lower ethane to methane ratios.

Abstract

There has been increasing interest in quantifying methane emissions from a view towards mitigation. Accordingly, ground-based sampling of oil and gas production sites in the Permian Basin was carried out in January and October 2020. Ethane to methane ratios (EMRs) were quantified which may be used to distinguish emissions from particular sources, such as produced gas and oil tank flashing. The logarithmic mean EMR for 102 observations was 18 (±2)%, while source specific EMRs showed that sites where emissions were attributed to a tank produced much higher EMRs averaging 44%. Sites with other noticeable sources such as compressors, pneumatics, and separators had lower and less variable EMRs. Tanks displayed distinct behavior with EMRs between 10-21% producing CH_4 emissions >30x higher than tanks with EMRs >21%. This observation supports the hypothesis that high emission rate tank sources are often caused by separator malfunctions that leak produced gas through liquids storage tanks.

Plain Language Summary

There has been increasing interest in quantifying methane emissions from a view towards mitigation. One sector of particular interest is oil and gas. To that end, a sampling campaign was deployed in the Permian Basin, one of the largest oil and gas production sites in the US that has seen an increase in the production of associated gas since 2006. We quantified the ratio of ethane co-emitted with methane and found that this ratio showed variability associated with the different production sources on site. One source (oil and condensate tanks) had an elevated ratio, relative to other noticeable sources. Tanks also displayed behavior where higher ratios were associated with lower methane emissions. This suggests that methane emissions from tanks are a result of abnormal conditions (such as separator malfunctions that leak produced gas through liquids storage tanks) and ethane to methane ratios may be used to identify such tanks.

1. Introduction

There has been considerable increase in oil and natural gas (ONG) production in the U.S. in the past decade that creates the possibility of an increase in associated methane (CH_4) emissions, which numerous studies have noted (Alvarez et al., 2018; Franco et al., 2016; Hausmann et al., 2016; Helmig et al., 2016; Nisbet et al., 2019; Raimi, 2019; Schneising et al., 2014). The Permian Basin in Texas and New Mexico covers more than 75,000 square miles (EIA, 2020). It is the largest oil producing shale formation in the US with 5,208 thousand barrels/day of oil and 20,280 million cubic feet per/day of NG as of April 2022 (EIA, 2022). Hence, there has been interest to quantify and mitigate the CH_4 emissions from this region. A recent ground-based study reported well-pad CH_4 emissions in the Permian 5-9 times higher than EPA inventory estimates (Robertson et al., 2020). Airborne and satellite analysis has also produced CH_4 emission rates that are also higher the inventory estimates (Chen et al., 2022; Irakulis-Loitxate et al., 2021; Schneising et al., 2020; Zhang et al., 2020). Recent work to constrain total CH_4 emissions from the Permian Basin have reported emissions from the production sector contributing ~50% of the total basin emissions (Chen et al., 2022; Cusworth et al., 2021). These studies also suggest that the largest emissions are well above the emission range seen from ground campaigns but could not distinguish the on-site source of emissions in most cases, though intermittent flares were identified as contributing 12% of emissions (Cusworth et al., 2021). Ground-based samples require large sample sizes to catch these 'super-emitters', which are infrequent and/or short-lived and have a low probability of being randomly sampled (Wang et al., 2022). Additionally, sources with lofted plumes (such as flares) may be impossible to quantify via ground-based methods if the plume remains above the measurement height.

The production sector includes well pads and tank batteries where a typical ONG well pad may consist of oil derricks or wellheads, compressors, crude or condensate tanks, produced water tanks, pneumatic controllers, and flaring units (EIA, 2021). Some of the routine activities like venting, use of pneumatic controllers, unintentional leakages, malfunctioning flaring units, and storage tanks contribute to the overall emissions from the production sector (Allen et al., 2022, 2015a, 2015b; Tyner & Johnson, 2021; Zimmerle et al., 2022). One method to identify a specific CH_4 source is by measuring a tracer gas emitted along with CH_4 such as ethane (C_2H_6). C_2H_6 is primarily emitted from ONG sources and thus has been used as a suitable tracer to

distinguish ONG emissions from other sources such as livestock (Peischl et al., 2018; Pollack et al., 2022; Smith et al., 2015).

Previous work has provided limited differentiated ethane to methane ratios (EMRs) for specific sources of various types of fossil fuel extraction and refining (Yacovitch et al., 2014, 2017, 2020). More commonly, EMRs are reported for large areas. Kort et al., (2016) determined the C_2H_6 emissions and the EMR from the Bakken shale region in North Dakota using aircraft measurements. Similarly, using airborne CH_4 and C_2H_6 measurements, Smith et al., (2015) determined EMRs for the microbial, low C_2H_6 fossil, and high C_2H_6 fossil sources in the Barnett Shale region in Texas. Peischl et al., (2018) characterized CH_4 and C_2H_6 fluxes for several ONG regions around the U.S. Both Peischl et al., (2018) and Smith et al., (2015) were able to quantify ONG CH_4 emissions in regions of mixed sources and demonstrate the use of these EMRs in constraining their results. More recently, estimates of EMRs for different oil-bearing and dry gas regions were used to identify the importance of oil reservoirs (like the Permian) as dominant sources of CH_4 among ONG activities (Tribby et al., 2022).

EMRs for specific ONG processes may be expected to change with geology, which affects the initial gas composition and can be quite variable (Tzompa-Sosa et al., 2017). Downstream of the production sector, the EMR of gas is lowered as ethane and other natural gas liquids are separated and the processed gas (>95% CH_4) is sent via the transmission sector to customers (API, 2021). Flaring may lower the EMR from the source gas as ethane is expected to combust more efficiently than methane, but this will depend on meteorology, gas exit velocity, and flame stability (API, 2021; Leahey et al., 2001). At many sites, produced water, condensate, and oil containing dissolved gases are stored on site in tanks at near-atmospheric pressure after being passed through a high-pressure separator that separates natural gas from liquids. The tanks periodically vent as pressure exceeds a set point, causing a quick release of the dissolved gas. These emissions are known as tank 'flashing' and the EMR will be a function of the dissolved gas concentrations and each species' solubility, which is affected by temperature and pressure (API, 2021); crude and condensate tank flashing typically has higher EMRs than the associated produced gas (Cardoso-Saldana et al., 2021). This study focuses on the use of ethane as a tracer to differentiate sources within the production sector in the Permian Basin. We measured C_2H_6 concentrations simultaneously with CH_4 and calculated site specific EMRs that were then assigned to the identified emitting sources on site.

2. Methods and Data processing

Using the University of Wyoming mobile lab (Robertson et al., 2017), two sampling campaigns were completed in January 2020 and October-November 2020. ONG sites in the Permian Basin in Texas and New Mexico were sampled. The region sampled primarily covered the Delaware Basin, which is the western portion of the Permian Basin. A map of the sampled locations is provided in Figure S2.

2.1. Data Collection

The University of Wyoming mobile lab included a 2D weather station, 3D sonic anemometer, and an inlet mounted 4 m above the ground connected to a gas sampling manifold. Inside the van, a 2Hz Picarro Cavity Ring-Down Spectrometer (CRDS, Model G2204) was used to measure CH_4 by sampling from the manifold. C_2H_6 measurements were also collected from the manifold using an Aerodyne Ethane-Mini spectrometer, a tunable infrared laser direct absorption spectroscopy instrument (QC-TILDAS), which has a frequency of 1 Hz (Yacovitch et al., 2014). The Picarro CRDS was calibrated using a high-precision standard CH_4/C_2H_6 air mixture created by the WMO/GAW Central Calibration Laboratories at NOAA's Global Monitoring Division with 1936.3 ± 0.2 ppb CH_4 and 2.09 ± 0.01 ppb C_2H_6. This was carried out twice throughout the sampling campaign. The reported precision for the CH_4 measurements was 2 ppb in 5s and the reading was always within 2.5 ppb of the standard. Similarly, for the calibration of Aerodyne Ethane-Mini spectrometer, the CH_4/C_2H_6 air mixture was used and the instrument was zeroed every 30 minutes using ultra high-purity zero air. The calculated precision for the C_2H_6 measurements was 80 ppt in 1s and the reading was always within 0.3 ppb of the standard.

As part of the Environmental Defense Fund's Permian Methane Analysis Project (PermianMAP), this campaign was designed to capture data suitable for CH_4 emission calculations using OTM 33A (Brantley et al., 2014; US-EPA 2014, 2014). Accordingly, OTM 33A data was collected while the van was stationary and downwind of a source for at least 20 mins. Optical gas imaging using a FLIR camera (model GF300) was taken during sampling and whenever possible the source of emissions was noted. Occasionally during this campaign transects were driven downwind of sources suitable for emission calculation by transect method (Caulton et al., 2018). The OTM 33A and transect data were used to calculate EMRs, which is the focus of this work.

133 2.2. Data Processing

134 Ratios were calculated by least squares regression between the CH_4 and C_2H_6 mixing
135 ratios where the slope of the fit represents the EMR. The reported 95% confidence interval (CI)
136 for each ratio is calculated from the uncertainty of the slope. These ratios are expressed as a
137 percentage of the CH_4 mixing ratio (ppb/ppb ×100). Ratios were screened to remove sites that
138 showed low correlation (R^2 value) between C_2H_6 and CH_4. The R^2 value used to screen out sites
139 was 0.65 (Yacovitch et al., 2014).

140 **3. Results and Discussion**

141 3.1. Sites with Multiple EMR Signatures

142 A few sites sampled (n=12) displayed two distinct EMR signals (Figure S1). Many of
143 these sites were initially screened out due to low correlation coefficients stemming from the fact
144 that a single fit could not represent the data. The EMR signatures can also be used to parse the
145 total CH_4 flux from the site into the contributions from individual signals, as detailed in the
146 Supplemental Information (SI). This calculation requires the total site CH_4 and C_2H_6 emissions
147 calculated either via OTM 33A or transect method and individual EMRs. Not all sites produced
148 two signals that passed the R^2 screening threshold and thus not all sites could be parsed. Analysis
149 of the wind direction data was used to identify the probable sources based on site notes and
150 photographs when possible. Results for this analysis are presented in Tables S1-S2. In general,
151 the few sites with multiple EMR signatures where one signal could be attributed to a tank
152 showed that non-tank sources typically were the largest CH_4 source. Further discussion of tanks
153 with respect to EMRs and CH_4 emission overall is presented in Section 3.2.

154 As an example of this process, we discuss Sites S02 and S03 measured on 22 Jan. 2020 in
155 more detail. These were repeat measurements of the same site and present a unique case study.
156 Prior to sampling, FLIR videos identified that the emissions coming from a separator and a tank,
157 which were about 65 m apart on the site. Pre-measurement transects showed consistent distinct
158 peaks for these sources (Figure S3). The initial sampling was oriented in the centerline of the
159 separator plume, and it was observed that the emission from the tank on site would not be fully
160 captured. The initial OTM 33A measurement (S02) was completed, and afterward the team
161 moved position to the centerline of the tank plume and completed another measurement (S03).

The low EMR is remarkably consistent between these sites (3.3% for S02 and 3.5% for S03). However, in S03 there is an additional signal observable in the data that returns an EMR of 21% coming from a tank. Additional analysis to corroborate the source signals and contributions are provided in the SI, which included using the transect plumes to calculate component emissions. Using the parsing method, the contribution of the total CH_4 emission from the tank to the S03 emission is small (7% of the total emission) and reasonably consistent with source specific emission estimates calculated from the transects (13% of the total emission).

This analysis of separate signals increased our sample size of screened EMRs from 88 to 102 and is used for the remainder of the analysis. These EMRs correspond to a unique site, or to a unique component on a site. There are at most two EMRs per site. The range of ratios calculated varied from 3.3% to 157%. Statistics of this dataset are reported using bootstrapping of 1000 samples with replacement. The mean and median ratios with 95% CIs were 26 (±6)% and 14 (±1)%, respectively. In addition, the logarithmic mean was calculated as 18 (±2)%. More than 50% of the observations had EMRs between 10-20%, which likely represents produced gas; however, we observed several ratios over 100% indicative of oil or condensate tank flashing. The distribution of EMRs displays right hand skewness (skew = 2.8). Figure S4 shows the distribution of EMRs on normal and lognormal axes.

3.2. Source Specific EMR Signatures

Sites were never sampled when operator activity was observed, thus no sources should represent maintenance activity or manual liquid unloadings. Bell et al., (2017) observed that OTM 33A underestimated sites from manual liquid unloadings, which contributed significant fractions of the total emissions in their sample. Though Bell et al., (2017) also noted underestimation of emissions from OTM 33A more recent work using controlled releases from a variety of well pad infrastructure generally showed good agreement, however, their release rates did not span above 2.15 kg hr^{-1} (Edie et al., 2020). Thus, we assume that the emissions estimates for these sites are robust and do not primarily contain sources that would have lofted plumes the ground sampling technique could not measure accurately. Sites were grouped by common source emission type for analysis of differences in EMRs. As sites can have multiple sources this analysis is not without some subjectivity, and it is possible that the identified source was not the only or primary source at a site. However, this procedure is consistent with the general way leaks

192 are detected via optical gas imaging (for example in Bell et al., (2017)) albeit without on-site
193 access. The team made observations by FLIR camera as close to the sources as possible from
194 publicly accessible land (typically at the edge of the well pad or road). The source categories
195 defined for this analysis included ‘compressor’, ‘pneumatics’, ‘separator’, and ‘tank’. A source
196 category contained any emission relating to that source type (e.g., tanks include any type of vent,
197 pipe or thief hatch on a tank and any type of tank: oil, condensate, produced water, saltwater).
198 Any site with more than one source noted was put into a ‘mixed signal’ category. Additionally,
199 some sites had no obvious source, or no information recorded at the time of sampling, and were
200 grouped together as ‘none/not identifiable’. Full details of the source observations from each site
201 are reported in Table S3. The results of this analysis are shown in Figure 2 with statistics
202 reported in Table S4.
203
204

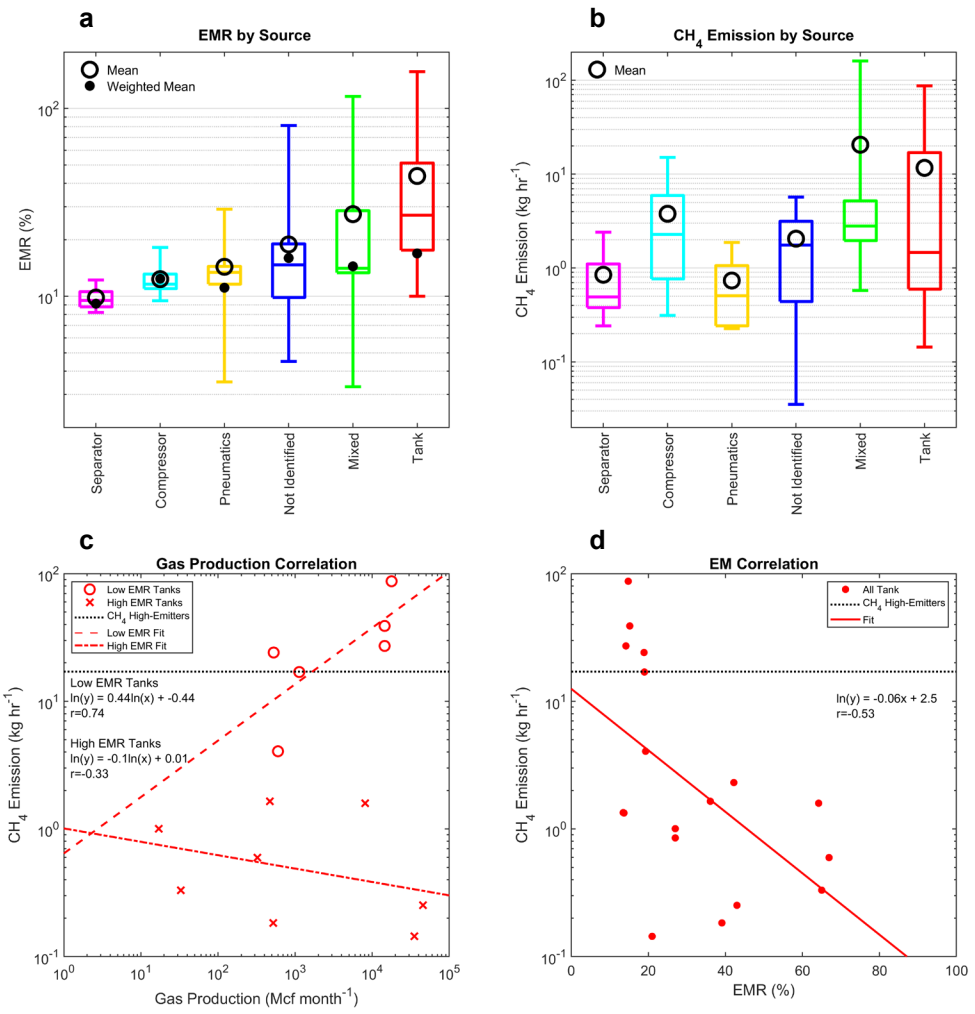

Figure 2. Box plots showing results of all sampled sites for (a) the EMR and (b) the CH_4 emission by source type. Box plots show the 25th, 50th, and 75th percentiles with the minimum and maximum data represented by the capped lines (no data is excluded as an outlier). In panel (a) the mean is shown an open black dot and the emission weighted mean (Eq. 1) as a filled black dot. Panel (c) shows the regression between CH_4 emission and monthly gas production for tank sites with low and high EMRs. The delineation of HEs is shown as the dotted black line. Panel (d) shows the regression plot between EMR and CH_4 emissions for tank sources along with the fit for the data in the solid red line.

There is a clear increase in average EMR for sites that have only tank emissions. This is consistent with observations that have reported high EMRs from tanks and processing equipment of wet-gas regions (Goetz et al., 2015, 2017; Yacovitch et al., 2014). In addition, data has shown

enhancement of alkane emissions from tank venting and flashing, through modeling and measurements (Cardoso-Saldana et al., 2021; Pétron et al., 2012). Mixed signals also show an elevated mean EMR. Most of the sites with mixed signals included at least one tank source so it is reasonable to assume that the mixed signal EMR is enhanced from the presence of tanks. These source categories also showed a large range in EMRs as seen from their large standard errors (Table S4). Comparatively, compressors, separators, and pneumatics had relatively consistent and lower EMRs. The sites with no identified source information also showed elevated EMR signals and higher variability, like the mixed signal category. Though there is a broad range of EMRs in the sample, most (>70%) of the sites had ratios <21%. For the 30 observations with EMRs ≥21%, 17 were directly attributed to tanks, six to sites with mixed signals where tanks were present, two to pneumatics, and five were not identifiable. All six sites with EMRs over 100% came from tanks or mixed signals where tanks were present. We also sampled a ground/pipeline leak (EMR = 13.7%) and an isolated flare emission (EMR = 16.3%).

Generally, sites with sources identified as tanks or mixed signals also had higher CH_4 emissions, but the range of CH_4 emission observations is larger than the range of EMRs. Also shown in Figure 2 and reported in Table S4 are emission weighted mean EMRs. This is calculated by multiplying the EMR in a source category by that site's CH_4 emission divided by the total CH_4 emissions from that category and summing the individual contributions, as shown in Eq. 1:

$$Weighted\ Mean\ EMR = \sum_{i=1}^{n} EMR(i) \times \frac{CH_4(i)}{CH_4\ Total} \quad \text{Eq. 1}$$

Some source categories show consistency between the mean and weighted mean EMR including compressors, pneumatics, separators, and even the category where sources were not identifiable. Mixed signals and tanks, however, show the largest difference between the mean and weighted mean. Tanks in particular have a very high mean (44%) and comparatively low weighted mean (17%). This suggests that while high EMRs indicate the presence of a tank, the tanks that cause high emissions do not have high EMRs. For the purpose of this analysis, we have defined 'high-emitters' (HEs) as sites with a CH_4 emission 10 × the logarithmic mean of the CH_4 emissions of this dataset (HE > 17 kg hr^{-1}). This value is not meant to be a universal standard, and all but one of the sites measured had CH_4 emission rates < 100 kg hr^{-1}. This procedure identified seven sites or ~10% of the dataset of CH_4 emissions as HEs. For tanks with EMR values ≥21%, none of the emissions can be classified as HEs. All the tanks associated with

HEs in this data set had EMRs between 10-21%. The mean CH_4 emission rate for these low EMR tanks (n=8) was over 30 times higher and statistically different from than the mean CH_4 emission rate for tanks with high EMRs (n=12). Statistics for the tanks broken up by EMR are reported in Table S5.

To explain these observations, we theorize that the high EMRs represent normal tank operations (e.g., flashing, working, and standing losses) that do not appear to be primarily associated with high emissions. Rather, the high CH_4 emissions may occur during abnormal conditions where separator or other issues pass unprocessed gas directly to the tank where it can leak to the atmosphere. This hypothesis is supported by other work that has suggested emissions from ONG primarily arise from abnormal conditions (Alvarez et al., 2018; Luck et al., 2019; Daniel Zavala-Araiza et al., 2017). The precise source of the abnormal condition may be similar or related to a known emission point from separator dump valves, which are used to release accumulated liquids and can become stuck open due to debris or other issues (API, 2021).

There is little direct support for this theory without on-site reports of equipment status. In the absence of such data, we have looked at site characteristics for further evidence. Not all of the low EMR tanks produced large CH_4 emissions. If these low EMR tanks primarily represent abnormal conditions, one factor limiting the amount of CH_4 that can be emitted is the amount of produced gas. Generally, there has been little evidence for significant relationships between gas production and site-level CH_4 emissions and we assume that most sites in these studies were operating normally; thus for normally operating sites we expect a moderate to weak relationship between these parameters (Brantley et al., 2014; Lyon et al., 2016; Omara et al., 2016; D. Zavala-Araiza et al., 2018). We separated the tanks by low and high EMR and regressed them against the gas production corresponding to the month of measurement to investigate the significance of these relationships. The results of this analysis are shown in Figure 2. Low EMR tanks showed a positive correlation ($r = 0.74$) between the natural log of monthly gas production and CH_4 emissions. However, the slope of this fit is not statistically different from 0. On the other hand, the regression between the natural log of monthly gas production and CH_4 emissions for high EMR tanks shows weak negative correlation ($r=-0.33$). For reference, the entire data set showed weak correlation between there parameters ($r = 0.11$). Following this analysis, the identification of HEs from tanks from this data set is consistently predicted by the presence of a

low EMR and high gas production value. More observations are needed to corroborate this theory, particularly with sites with even higher CH_4 emission rates (>100 kg hr^{-1}).

We caution that as subcategories are further divided, the number of observations in any category becomes increasingly small and prone to spurious relationships. It should also be noted that there is no evidence for a direct correlation between EMR and CH_4 emissions. Using a regression of the calculated ratios versus the calculated OTM 33A or transect CH_4 emissions (n=65), we found a Pearson correlation coefficient of -0.1. The correlation is only statistically significant ($p<0.05$) for tanks with a correlation coefficient of -0.53 (Figure 2). However, there appears to be two distinct regions to the tanks EMR vs CH_4 correlation corresponding to the 21% EMR threshold previously identified. Complicating this analysis is the fact that the CH_4 distribution of this dataset is more positively skewed (skew = 5.1) than the EMR distribution (skew = 2.8). This is consistent with observations of CH_4 emissions from ONG operations that show extreme right skew behavior, which has been observed in the Permian as well (Brandt et al., 2016; Robertson et al., 2020). The presence of HEs that occur at low frequency has the effect of substantially altering the mean of any data set. Therefore, it is appropriate to use caution when interpreting trends associated with these extremes. The conclusion that tanks have statistically higher mean EMRs than any other identified source is robust and consistent with previous observations (Cardoso-Saldana et al., 2021; Goetz et al., 2015, 2017). The observation that tanks with low EMRs have on average higher CH_4 emissions than tanks with high EMRs is also statistically robust, and a novel finding of this work. The interpretation that there is a direct relationship between gas production and CH_4 emission for low EMR tanks, and an inverse relationship between EMR and CH_4 emission from tanks requires more observations to corroborate because HEs occur infrequently and can dramatically alter the regressions.

3.3. Regional EMR

As mentioned, the range of EMRs observed in this data produced a skewed distribution. This distribution yielded a range of statistics with different values, as stated earlier, with a mean, median and logarithmic mean of 26 (±6)%, 14 (±1)%, and 18 (±2)%, respectively. This gives rise to the question of which statistic is most appropriate for comparison to other literature or useful for other analysis. Because the uncertainty on most of the statistics was relatively high, we also calculated a regional EMR through regression analysis of the background concentration data

collected when transiting between sites. For this analysis, background data was calculated as a running mean of the lowest 30% of the data in 30s bins, which removed sharp peaks, but preserved large scale variations in the background. Some results of this procedure are show in Figure S5. The background data was then regressed to produce an EMR that should be representative of the weighted EMR for the region including sectors other than production. However, because this area was dominated by production sites, the ratio is expected to be similar to the production sector. We also separated the data based on the season of measurement to observe temporal trends in the EMR. The EMR ranged from 16.77 (±0.02)% in winter to 18.98 (±0.03)% the following fall with a combined ratio of 17.3 (±0.2)% (Figure S6). There is some overlap in the sampling area between the winter and fall campaigns though the area is not exactly the same (Figure S2). The logarithmic mean of the production sector EMRs (18%) compares best with the regression EMR for the region and may be the best statistic to represent skewed EMR distributions.

An additional vector of comparison can be made using available gas composition data. (Kort et al., 2016) found that their EMR was consistent with the composition of NG production data from 710 sites in the Bakken Shale which had an EMR of 42%. Peischl et al., (2018) also reported C_2H_6 and CH_4 fluxes for several regions and compared to available gas composition data in those regions and generally found good agreement. This previous work suggests that gas composition may be used as a proxy for expected EMRs from production sites. For this study, we compared our results to the gas composition statistics from 19 wells in the Permian Basin (ERG, 2012; Fairhurst & Hanson, 2012; Howard et al., 2015). The bootstrapped statistics for the gas composition mean and median EMR are 13 (±3)% and 15 (±6)%, respectively. The gas composition mean EMR is statistically lower than the mean ratio calculated from this study of 26%. It is also slightly lower (and statistically different) than the regional EMR (17.3%) and logarithmic mean (18%). The median gas composition EMR is more uncertain, but compares better with the site EMR statistics and regional EMR calculated in this study. The gas composition data used in this analysis primarily came from wells in Texas in both the Delaware and Midland basins, which span a wide geographical area and include areas outside of our study region (Figure S2). Large datasets of gas composition are not always readily available (as in this case) and composition varies from well to well, thus comparison to a few wells is not very meaningful. The gas composition EMR from the available data varied from <1% to 24% and was

not normally distributed. In addition, the results presented here show that the surface source types do not have uniform EMRs suggesting it is more appropriate to actually measure EMRs than assume gas composition is an equivalent metric.

4. Implications

This study presented calculations of EMRs from 102 screened observations. We observed a logarithmic mean ratio of 18 (±2)% for these production sites measured in the Permian basin that compares well to a regional EMR of 17.3 (±0.2)%. Component specific EMRs were calculated with tanks producing the highest average EMR at 44%. Tanks also displayed distinct behavior in CH_4 emissions for sites that were close to the regional EMR (10-21%) and sites that had elevated EMRs (21-157%). The highest CH_4 emissions from tanks in this dataset had lower EMRs and high gas production values. Of the five highest emitting sites in this study, which contributed 75% of emissions, four sites were categorized as tanks and one as a mixed signal. However, none of these sites had EMRs over 21%. The observation that tanks are a primary source of elevated CH_4 emission rates in this dataset is consistent with recent observations that also identify tanks as a major source of CH_4 emissions (Tyner & Johnson, 2021).

We have put forth a hypothesis for these observations which implies that the elevated CH_4 emissions from tanks are mainly from produced gas escaping through the tank, rather than tank flashing. This indicates these high tank CH_4 emissions are driven by abnormal conditions and perhaps caused by or related to separator issues such as a stuck dump valve. Therefore, EMRs could have use for determining when detected emissions are normal vs abnormal. EMRs are computationally easy as they can be calculated directly from concentration measurements and do not rely on meteorology. We used ~20 minutes of data for these calculations, but we were also able to calculate EMRs from aborted OTM 33A measurements and transects that lasted only a few minutes. It may be possible to quickly quantify the EMR from tanks to determine whether they are behaving abnormally and implement remediation, regardless of gas production value. Gas production value may have use for optimizing such a strategy to target high CH_4 emission sites.

In addition to distinguishing production sources, EMRs may have use in defining the contribution of sector emissions at large scales. Though previous work has shown that the mean EMR is generally close to the gas composition of the region (Kort et al., 2016; Peischl et al.,

2015, 2018), this work showed that EMRs varied by source, suggesting raw gas composition data is not an accurate representation of the surface emission EMRs, especially in areas that have equipment such as tanks (i.e., wet gas/associated gas regions). Other recent work has made an argument against using gas composition in regions where transmission sector equipment produces lower EMRs than expected by gas composition data (Zimmerle et al., 2022). In addition, measurements of processing equipment have shown a range or EMRs and even scenarios where C_2H_6 is released without CH_4 (Roscioli et al., 2015; Yacovitch et al., 2014, 2015). This illustrates the likely variability of EMR signatures across sectors in addition to regional differences. Cusworth et al., (2021) estimated the distribution of emissions based on sector in the Permian in 2019. It may be possible to corroborate such contributions from different sectors using C_2H_6 observations if they are associated with different mean EMRs. As Smith et al., (2015) showed, there is considerable uncertainty when attempting to use only C_2H_6 and CH_4 to partition signals in a region with multiple EMRs. Observations of other tracers, like CO_2 or H_2S may be necessary to fully implement such analysis.

Finally, the results presented here provide some implications for low-cost sensors, which have been gaining increasing attention as a cheap and large-scale monitoring solution (Riddick et al., 2022; Zhou et al., 2021). Because most low-cost sensors like photoionization detectors (PIDs) are not very selective, they may be prone to producing false high emission rates when they are in the plume of a tank, due to the presence of interfering hydrocarbons. This could lead to consistent 'false positive' reading for tank emissions and limit the efficiency of leak detection from PIDs.

Acknowledgments

The authors declare no competing financial interests. This work was funded by the Environmental Defense Fund as part of the Permian Methane Analysis Project (PermianMAP) campaign. PermianMAP, which includes the aerial, tower, and flare survey data, is grateful for the support of Bloomberg Philanthropies, Grantham Foundation for the Protection of the Environment, High Tide Foundation, the John D. and Catherine T. MacArthur Foundation, Quadrivium, and the Zegar Family Foundation. The School of Energy Resources at the University of Wyoming also provided financial support for the mobile lab, instrumentation and students. We would like to thank Megan McCabe for help in data collection during the January

'20 campaign, Matt Burkhart and Zane Little for technical support and maintenance of the mobile lab and Jack Warren for help in obtaining and aggregating the gas production data from Enverus.com.

CRediT Author Statement

- D.R.C.: Supervision, Conceptualization, Visualization, Writing-Original Draft
- P.D.G.: Formal analysis, Data curation, Writing-Reviewing and Editing
- A.M.R.: Project administration, Formal analysis, Data Curation, Writing-Reviewing and Editing
- K.P.: Data Curation
- S.M.R.: Funding Acquisition, Conceptualization, Writing-Reviewing and Editing
- D.R.L.: Writing-Reviewing and Editing

Open Research

The data containing EMRs, CH_4 emissions and supporting information will be made available at https://data.permianmap.org/. This data repository is maintained by the Environmental Defense Fund and is free and open to the public with agreement to abide by the terms of use, which are available at the website.

References

Allen, D. T., Sullivan, D. W., Zavala-Araiza, D., Pacsi, A. P., Harrison, M., Keen, K., et al. (2015a). Methane emissions from process equipment at natural gas production sites in the United States: Liquid unloadings. *Environmental Science and Technology*, *49*(1), 641–648. https://doi.org/10.1021/es504016r

Allen, D. T., Pacsi, A. P., Sullivan, D. W., Zavala-Araiza, D., Harrison, M., Keen, K., et al. (2015b). Methane emissions from process equipment at natural gas production sites in the United States: Pneumatic controllers. *Environmental Science and Technology*, *49*(1), 633–640. https://doi.org/10.1021/es5040156

Allen, D. T., Cardoso-Saldaña, F. J., Kimura, Y., Chen, Q., Xiang, Z., Zimmerle, D., et al. (2022). A Methane Emission Estimation Tool (MEET) for predictions of emissions from upstream oil and gas well sites with fine scale temporal and spatial resolution: Model structure and applications. *Science of the Total Environment*, *829*. https://doi.org/10.1016/j.scitotenv.2022.154277

Alvarez, R. A., Zavala-Araiza, D., Lyon, D. R., Allen, D. T., Barkley, Z. R., Brandt, A. R., et al. (2018). Assessment of methane emissions from the U.S. oil and gas supply chain. *Science*, *361*(6398), 186–188. https://doi.org/10.1126/science.aar7204

API. (2021). *COMPENDIUM OF GREENHOUSE GAS EMISSIONS METHODOLOGIES FOR THE NATURAL GAS AND OIL INDUSTRY COMPENDIUM OF GREENHOUSE GAS EMISSIONS METHODOLOGIES FOR THE NATURAL GAS AND OIL INDUSTRY*.

Bell, C. S., Vaughn, T. L., Zimmerle, D., Herndon, S. C., Yacovitch, T. I., Heath, G. A., et al. (2017). Comparison of methane emission estimates from multiple measurement techniques at natural gas production pads. *Elementa Science of the Anthropocene*, *5*. https://doi.org/10.1525/elementa.266

Brandt, A. R., Heath, G. a., & Cooley, D. (2016). Methane Leaks from Natural Gas Systems Follow Extreme Distributions. *Environmental Science and Technology*, *50*(22), 12512–12520. https://doi.org/10.1021/acs.est.6b04303

Brantley, H. L., Thoma, E. D., Squier, W. C., Guven, B. B., & Lyon, D. (2014). Assessment of Methane Emissions from Oil and Gas Production Pads using Mobile Measurements. *Environmental Science and Technology*, *48*(24), 14508–14515. https://doi.org/10.1021/es503070q

448 Cardoso-Saldana, F. J., Pierce, K., Chen, Q., Kimura, Y., & Allen, D. T. (2021). A searchable
449 database for prediction of emission compositions from upstream oil and gas sources.
450 *Environmental Science and Technology*, *55*(5), 3210–3218.
451 https://doi.org/10.1021/acs.est.0c05925
452 Caulton, D. R., Li, Q., Bou-Zeid, E., Lu, J., Lane, H. M., Fitts, J. P., et al. (2018). Quantifying
453 uncertainties from mobile-laboratory-derived emissions of well pads using inverse Gaussian
454 methods. *Atmospheric Chemistry and Physics*, *18*(20), 15145–15168.
455 https://doi.org/10.5194/acp-18-15145-2018
456 Chen, Y., Sherwin, E. D., Berman, E. S. F., Jones, B. B., Gordon, M. P., Wetherley, E. B., et al.
457 (2022). Quantifying Regional Methane Emissions in the New Mexico Permian Basin with a
458 Comprehensive Aerial Survey. *Environmental Science & Technology*, *56*(7), 4317–4323.
459 https://doi.org/10.1021/acs.est.1c06458
460 Cusworth, D. H., Duren, R. M., Thorpe, A. K., Olson-Duvall, W., Heckler, J., Chapman, J. W.,
461 et al. (2021). Intermittency of Large Methane Emitters in the Permian Basin. *Environmental*
462 *Science and Technology Letters*, *8*(7), 567–573. https://doi.org/10.1021/acs.estlett.1c00173
463 Eastern Research Group. (2012). *APPENDIX C: CONDENSATE TANK OIL AND GAS*
464 *ACTIVITIES*. Austin, TX.
465 Edie, R., Robertson, A. M., Soltis, J., Field, R. A., Snare, D., Burkhart, M. D., & Murphy, S. M.
466 (2020). Off-Site Flux Estimates of Volatile Organic Compounds from Oil and Gas
467 Production Facilities Using Fast-Response Instrumentation. *Environmental Science and*
468 *Technology*, *54*(3), 1385–1394. https://doi.org/10.1021/acs.est.9b05621
469 EIA. (2020). *Permian Basin Part 2 Wolfcamp Shale Play of the Midland Basin Geology review:*
470 *U.S. Energy Information Administration.* Retrieved from
471 https://www.eia.gov/maps/pdf/Permian_Wolfcamp_Midland_EIA_reportII.pdf.
472 EIA. (2021, December 2). Natural Gas Explained.
473 EIA. (2022). *Drilling Productivity Report*. Retrieved from
474 https://www.eia.gov/petroleum/drilling/
475 Fairhurst, B., & Hanson, M. L. (2012). *Evolution and Development of the WolfBone Play,*
476 *Southern Delaware Basin, West Texas: An Emerging Frontier, An Oil-Rich Unconventional*
477 *Resource #10411*.

Franco, B., Mahieu, E., Emmons, L. K., Tzompa-Sosa, Z. A., Fischer, E. v., Sudo, K., et al. (2016). Evaluating ethane and methane emissions associated with the development of oil and natural gas extraction in North America. *Environmental Research Letters*, *11*(4). https://doi.org/10.1088/1748-9326/11/4/044010

Fritz, B. K., Shaw, B. W., & Parnell, C. B. (2005). INFLUENCEOF METEOROLOGICAL TIME FRAMEANDVARIATIONON HORIZONTAL DISPERSION COEFFICIENTSIN GAUSSIAN DISPERSION MODELING. *Transactions of the American Society of Agricultural Engineers*, *48*(3), 1185–1196. https://doi.org//10.13031/2013.18501

Goetz, J. D., Floerchinger, C., Fortner, E. C., Wormhoudt, J., Massoli, P., Knighton, W. B., et al. (2015). Atmospheric emission characterization of marcellus shale natural gas development sites. *Environmental Science and Technology*, *49*(11), 7012–7020. https://doi.org/10.1021/acs.est.5b00452

Goetz, J. D., Avery, A., Werden, B., Floerchinger, C., Fortner, E. C., Wormhoudt, J., et al. (2017). Analysis of local-scale background concentrations of methane and other gas-phase species in the Marcellus Shale. *Elementa Science of the Anthropocene*, *5*, 1–20. https://doi.org/10.1525/elementa.182

Hausmann, P., Sussmann, R., & Smale, D. (2016). Contribution of oil and natural gas production to renewed increase in atmospheric methane (2007-2014): Top-down estimate from ethane and methane column observations. *Atmospheric Chemistry and Physics*, *16*(5), 3227–3244. https://doi.org/10.5194/acp-16-3227-2016

Helmig, D., Rossabi, S., Hueber, J., Tans, P., Montzka, S. A., Masarie, K., et al. (2016). Reversal of global atmospheric ethane and propane trends largely due to US oil and natural gas production. *Nature Geoscience*, *9*(7), 490–495. https://doi.org/10.1038/ngeo2721

Howard, T., Ferrara, T. W., & Townsend-Small, A. (2015). Sensor transition failure in the high flow sampler: Implications for methane emission inventories of natural gas infrastructure. *Journal of the Air and Waste Management Association*, *65*(7), 856–862. https://doi.org/10.1080/10962247.2015.1025925

Irakulis-Loitxate, I., Guanter, L., Liu, Y.-N., Varon, D. J., Maasakkers, J. D., Zhang, Y., et al. (2021). Satellite-based survey of extreme methane emissions in the Permian basin. *Science Advances*, *7*(27), 1–8. https://doi.org/10.1126/sciadv.abf4507

Kort, E. A., Smith, M. L., Murray, L. T., Gvakharia, A., Brandt, A. R., Peischl, J., et al. (2016). Fugitive emissions from the Bakken shale illustrate role of shale production in global ethane shift. *Geophysical Research Letters*, *43*(9), 4617–4623. https://doi.org/10.1002/2016GL068703

Leahey, D. M., Preston, K., & Strosher, M. (2001). Theoretical and observational assessments of flare efficiencies. *Journal of the Air and Waste Management Association*, *51*(12), 1610–1616. https://doi.org/10.1080/10473289.2001.10464390

Luck, B., Zimmerle, D., Vaughn, T., Lauderdale, T., Keen, K., Harrison, M., et al. (2019). Multiday Measurements of Pneumatic Controller Emissions Reveal the Frequency of Abnormal Emissions Behavior at Natural Gas Gathering Stations. *Environmental Science and Technology Letters*, *6*(6), 348–352. rapid-communication. https://doi.org/10.1021/acs.estlett.9b00158

Lyon, D. R., Alvarez, R. A., Zavala-Araiza, D., Brandt, A. R., Jackson, R. B., & Hamburg, S. P. (2016). Aerial Surveys of Elevated Hydrocarbon Emissions from Oil and Gas Production Sites. *Environmental Science and Technology*, *50*(9), 4877–4886. https://doi.org/10.1021/acs.est.6b00705

Nisbet, E. G., Manning, M. R., Dlugokencky, E. J., Fisher, R. E., Lowry, D., Michel, S. E., et al. (2019). Very Strong Atmospheric Methane Growth in the 4 Years 2014–2017: Implications for the Paris Agreement. *Global Biogeochemical Cycles*, *33*(3), 318–342. https://doi.org/10.1029/2018GB006009

Omara, M., Sullivan, M. R., Li, X., Subramian, R., Robinson, A. L., & Presto, A. A. (2016). Methane Emissions from Conventional and Unconventional Natural Gas Production Sites in the Marcellus Shale Basin. *Environmental Science and Technology*, *50*(4), 2099–2107. https://doi.org/10.1021/acs.est.5b05503

Peischl, J., Ryerson, T. B., Aikin, K. C., Gouw, J. A., Gilman, J. B., Holloway, J. S., et al. (2015). Quantifying atmospheric methane emissions from the Haynesville, Fayetteville, and northeastern Marcellusshale gas production regions. *Journal of Geophysical Research: Atmospheres*, (120), 2119–2139. https://doi.org/10.1002/2014JD022697

Peischl, J., Eilerman, S. J., Neuman, J. A., Aikin, K. C., de Gouw, J., Gilman, J. B., et al. (2018). Quantifying Methane and Ethane Emissions to the Atmosphere From Central and Western

U.S. Oil and Natural Gas Production Regions. *Journal of Geophysical Research: Atmospheres*, *123*(14), 7725–7740. https://doi.org/10.1029/2018JD028622

Pétron, G., Frost, G., Miller, B. R., Hirsch, A. I., Montzka, S. A., Karion, A., et al. (2012). Hydrocarbon emissions characterization in the Colorado Front Range: A pilot study. *Journal of Geophysical Research Atmospheres*. Blackwell Publishing Ltd. https://doi.org/10.1029/2011JD016360

Pollack, I. B., Mccabe, M. E., Caulton, D. R., & Fischer, E. v. (2022). Enhancements in Ammonia and Methane from Agricultural Sources in the Northeastern Colorado Front Range Using Observations from a Small Research Aircraft. *Environmental Science & Technology*, *56*(4), 2236–2247. https://doi.org/10.1021/acs.est.1c07382

Raimi, D. (2019). The Greenhouse Gas Impacts of Increased US Oil and Gas Production. Washington, DC: Resource for the Future.

Riddick, S. N., Ancona, R., Cheptonui, F., Bell, C. S., Duggan, A., Bennett, K. E., & Zimmerle, D. J. (2022). A cautionary report of calculating methane emissions using low-cost fence-line sensors. *Elementa: Science of the Anthropocene*, *10*(1). https://doi.org/10.1525/elementa.2022.00021

Robertson, A. M., Edie, R., Snare, D., Soltis, J., Field, R. A., Burkhart, M. D., et al. (2017). Variation in Methane Emission Rates from Well Pads in Four Oil and Gas Basins with Contrasting Production Volumes and Compositions. *Environmental Science and Technology*, *51*(15), 8832–8840. https://doi.org/10.1021/acs.est.7b00571

Robertson, A. M., Edie, R., Field, R. A., Lyon, D., McVay, R., Omara, M., et al. (2020). New Mexico Permian basin measured well pad methane emissions are a factor of 5−9 times higher than U.S. EPA estimates. *Environmental Science and Technology*, *54*(21), 13926–13934. https://doi.org/10.1021/acs.est.0c02927

Roscioli, J. R., Yacovitch, T. I., Floerchinger, C., Mitchell, A. L., Tkacik, D. S., Subramanian, R., et al. (2015). Measurements of methane emissions from natural gas gathering facilities and processing plants: Measurement methods. *Atmospheric Measurement Techniques*, *8*(5), 2017–2035. https://doi.org/10.5194/amt-8-2017-2015

Schneising, O., Burrows, J. P., Dickerson, R. R., Buchwitz, M., Reuter, M., & Bovensmann, H. (2014). Remote sensing of fugitive methane emissions from oil and gas production in North American tight geologic formations. *Earth's Future*, *2*(10), 548–558.

Schneising, O., Buchwitz, M., Reuter, M., Vanselow, S., Bovensmann, H., & P. Burrows, J. (2020). Remote sensing of methane leakage from natural gas and petroleum systems revisited. *Atmospheric Chemistry and Physics*, *20*(15), 9169–9182. https://doi.org/10.5194/acp-20-9169-2020

Smith, M. L., Kort, E. A., Karion, A., Sweeney, C., Herndon, S. C., & Yacovitch, T. I. (2015). Airborne Ethane Observations in the Barnett Shale: Quantification of Ethane Flux and Attribution of Methane Emissions. *Environmental Science and Technology*, *49*(13), 8158–8166. https://doi.org/10.1021/acs.est.5b00219

Tribby, A. L., Bois, J. S., Montzka, S. A., Atlas, E. L., Vimont, I., Lan, X., et al. (2022). Hydrocarbon Tracers Suggest Methane Emissions from Fossil Sources Occur Predominately Before Gas Processing and That Petroleum Plays Are a Significant Source. *Environmental Science & Technology*. https://doi.org/10.1021/acs.est.2c00927

Tyner, D. R., & Johnson, M. R. (2021). Where the Methane Is - Insights from Novel Airborne LiDAR Measurements Combined with Ground Survey Data. *Environmental Science and Technology*, *55*(14), 9773–9783. https://doi.org/10.1021/acs.est.1c01572

Tzompa-Sosa, Z. A., Mahieu, E., Franco, B., Keller, C. A., Turner, A. J., Helmig, D., et al. (2017). Revisiting global fossil fuel and biofuel emissions of ethane. *Journal of Geophysical Research*, *122*(4), 2493–2512. https://doi.org/10.1002/2016JD025767

US-EPA 2014. (2014). *SOP for Analysis of US EPA GMAP-REQ-DA Method Data for Methane Emission Rate Quantification using the Point Source Gaussian Method SOP 601 for OTM 33A*.

Wang, J., Daniels, W. S., Hammerling, D. M., Harrison, M., Burmaster, K., George, F. C., & Ravikumar, A. P. (2022). Multi-scale Methane Measurements at Oil and Gas Facilities Reveal Necessary Framework for Improved Emissions Accounting. *EarthArXiv*, 1–37. https://doi.org/10.26434/chemrxiv-2022-9zh2v

Yacovitch, T. I., Herndon, S. C., Roscioli, J. R., Floerchinger, C., McGovern, R. M., Agnese, M., et al. (2014). Demonstration of an ethane spectrometer for methane source identification. *Environmental Science and Technology*, *48*(14), 8028–8034. https://doi.org/10.1021/es501475q

Yacovitch, T. I., Herndon, S. C., Pétron, G., Kofler, J., Lyon, D., Zahniser, M. S., & Kolb, C. E. (2015). Mobile Laboratory Observations of Methane Emissions in the Barnett Shale

Region. *Environmental Science and Technology*, *49*(13), 7889–7895. https://doi.org/10.1021/es506352j

Yacovitch, T. I., Daube, C., Vaughn, T. L., Bell, C. S., Roscioli, J. R., Knighton, W. B., et al. (2017). Natural gas facility methane emissions: Measurements by tracer flux ratio in two US natural gas producing basins. *Elementa*, *5*(2013). https://doi.org/10.1525/elementa.251

Yacovitch, T. I., Daube, C., & Herndon, S. C. (2020). Methane Emissions from Offshore Oil and Gas Platforms in the Gulf of Mexico. *Environmental Science and Technology*, *54*(6), 3530–3538. https://doi.org/10.1021/acs.est.9b07148

Zavala-Araiza, D., Herndon, S. C., Roscioli, J. R., Yacovitch, T. I., Johnson, M. R., Tyner, D. R., et al. (2018). Methane emissions from oil and gas production sites in Alberta, Canada. *Elementa: Science of the Anthropocene*, *6*(27), 1–13. https://doi.org/10.1525/elementa.284

Zavala-Araiza, Daniel, Alvarez, R. A., Lyon, D. R., Allen, D. T., Marchese, A. J., Zimmerle, D. J., & Hamburg, S. P. (2017). Super-emitters in natural gas infrastructure are caused by abnormal process conditions. *Nature Communications*, *8*. https://doi.org/10.1038/ncomms14012

Zhang, Y., Gautam, R., Pandey, S., Omara, M., Maasakkers, J. D., Sadavarte, P., et al. (2020). Quantifying methane emissions from the largest oil-producing basin in the United States from space. *Science Advances*, *6*(17), 1–9. https://doi.org/10.1126/sciadv.aaz5120

Zhou, X., Peng, X., Montazeri, A., McHale, L. E., Gaßner, S., Lyon, D. R., et al. (2021). Mobile Measurement System for the Rapid and Cost-Effective Surveillance of Methane and Volatile Organic Compound Emissions from Oil and Gas Production Sites. *Environmental Science and Technology*, *55*(1), 581–592. https://doi.org/10.1021/acs.est.0c06545

Zimmerle, D., Duggan, G., Vaughn, T., Bell, C., Lute, C., Bennett, K., et al. (2022). Modeling air emissions from complex facilities at detailed temporal and spatial resolution: The Methane Emission Estimation Tool (MEET). *Science of the Total Environment*, *824*. https://doi.org/10.1016/j.scitotenv.2022.153653

Geophysical Research Letters

Supporting Information for

Identifying Abnormal Tank Emissions Using Ethane to Methane Signatures of Oil and Natural Gas Production in the Permian Basin

Dana R. Caulton[1], Priya D. Gurav[1], Anna. M. Robertson[1], Kristen Pozsonyi[1], Shane M. Murphy[1], David R. Lyon[2]

[1] Department of Atmospheric Science, University of Wyoming, Laramie, WY, USA.

[2] Environmental Defense Fund, Austin, TX, USA.

Corresponding author: Dana R. Caulton (dcaulton@uwyo.edu)

Contents of this file

Introduction

The supplemental information contains the following:

S1. Multiple EMR Signatures Parsing Method

This section describes the derivation of equations used to parse the total CH_4 emission to contributing sources from sites with two EMRs. In order to separate the EMR signals, principal component analysis (PCA) was performed. PCA was used to identify distinct groups which were subsequently analyzed separately. The results from an example of such an analysis are shown in Figure S1. Analysis of the wind direction data was used to identify the probable sources based on site notes and photographs when possible. Figure S1 shows an example of a site with distinct wind directions associated with each signal.

The following sections describes the system of equations used to solve for the individual fluxes. All fluxes are in units of mol/s and EMRs are in fractional form. Eqs. 1.1-1.4 represent the initial system of equations (4 equations, 4 unknowns). In Eq. 1.1 $F_{CH_4,T}$ is the total CH_4 flux at a given site, $F_{CH_4,A}$ is the CH_4 flux corresponding to signal A and $F_{CH_4,B}$ is the CH_4 flux corresponding to signal B. The analogous components of the total C_2H_6 flux ($F_{C_2H_6,T}$) are represented using A and B subscripts in Eq. 1.2. The ratio between the signal A and B C_2H_6 and CH_4 fluxes are constrained by the observed EMRs for signal A and B in Eqs. 1.3 and 1.4. Rearranging Eqs. 1.3 and 1.4 and substituting into 1.2 yields Eq. 2.1. Rearranging Eq. 2.1 to solve for $F_{CH_4,B}$ gives Eq. 2.2. Substituting Eq. 2.2 into Eq. 1.1 gives Eq. 3.1, which contains only one unknown, $F_{CH_4,A}$. Eqs. 3.2-3.4 show the process of solving for $F_{CH_4,A}$ and the final equation for $F_{CH_4,A}$ is given in Eq. 4. From this step, Eqs 1.1, 1.3 and 1.4 can be solved to produce all four unknowns.

$$F_{CH_4,A} + F_{CH_4,B} = F_{CH_4,T} \quad \text{Eq. 1.1}$$

$$F_{C_2H_6,A} + F_{C_2H_6,B} = F_{C_2H_6,T} \quad \text{Eq. 1.2}$$

$$\frac{F_{C_2H_6,A}}{F_{CH_4,A}} = EM_A \quad \text{Eq. 1.3}$$

$$\frac{F_{C_2H_6,B}}{F_{CH_4,B}} = EM_B \quad \text{Eq. 1.4}$$

$$F_{CH_4,A} \times EM_A + F_{CH_4,B} \times EM_B = F_{C_2H_6,T} \quad \text{Eq. 2.1}$$

$$F_{CH_4,B} = \frac{F_{C_2H_6,T} - F_{CH_4,A} \times EM_A}{EM_B} \quad \text{Eq. 2.2}$$

$$F_{CH_4,A} + \frac{F_{C_2H_6,T} - F_{CH_4,A} \times EM_A}{EM_B} = F_{CH_4,T} \quad \text{Eq. 3.1}$$

$$F_{CH_4,A} + \frac{F_{C_2H_6,T}}{EM_B} - \frac{F_{CH_4,A} \times EM_A}{EM_B} = F_{CH_4,T} \quad \text{Eq. 3.2}$$

$$F_{CH_4,A} - \frac{F_{CH_4,A} \times EM_A}{EM_B} = F_{CH_4,T} - \frac{F_{C_2H_6,T}}{EM_B} \quad \text{Eq. 3.3}$$

$$F_{CH_4,A}\left(1 - \frac{EM_A}{EM_B}\right) = F_{CH_4,T} - \frac{F_{C_2H_6,T}}{EM_B} \quad \text{Eq. 3.4}$$

$$F_{CH_4,A} = \frac{F_{CH_4,T} - \frac{F_{C_2H_6,T}}{EM_B}}{\left(1 - \frac{EM_A}{EM_B}\right)} \quad \text{Eq. 4}$$

Due to the assumptions that go into emission calculations combined with reliance on additional meteorological data, the error associated with emission calculation is much higher than the error associated with EMRs. This can result in situations where the site combined EMR as determined from the ratio of the molar C_2H_6 and CH_4 fluxes is higher or lower than should be possible. For example, Site 1030 S03 (see Table S1) has a flux EMR of 13.2% while the contributing signals from the regression analysis are 47% and 15.1%. The combined site EMR should be within these two limits. However, the error on the flux EMR is also large. By adding the expected OTM 33A error estimates calculated by Edie et al., (2020) in quadrature the resulting error on the flux EMR is +76%/-37%.

Error on the calculated CH_4 and C_2H_6 fluxes for signals A and B arises primarily from the error on the total flux calculations and the addition/subtraction terms. Errors from addition/subtraction are propagated by added the absolute error in quadrature, and thus will differ based on the magnitude of each site. As an example, the 95% CI on the CH_4 and C_2H_6 fluxes for 0122 S03 is ±177% for Signal A and ±52% for Signal B. In this case, the contribution of Signal A is not statistically significant. For 1030 S02 the 95% CI on the CH_4 and C_2H_6 fluxes is ±190% for Signal A and ±68% for Signal B. Again, Signal A is not statistically significant.

S2. Sites S02/S03 on 22 January 2020

This section presents further discussion of the case study on 22 January 2020 (Section 3.1 in the main text) where a site was measured twice, and the second measurement produced results with two EMR signals. The CH_4 emissions calculated by OTM 33A actually decreased from S02

to S03 by 16%. These emission rates are not ideal for comparison because Gaussian theory predicts that the signals for both sources should be partially mixed along the road. Because the tank signal is not observable in the S02 data, this emission rate may be attributable to the separator, however, it is also possible that the tank signal was diluted and impossible to distinguish from the dominant separator signal. S03 shows clear signal mixing so it does not solely represent the emission from the tank. Using the parsing method, the contribution of the total CH_4 emission from the tank to the S03 emission is small (7% of the total emissions). This suggests the repositioning to catch the tank signal excluded some of the overall CH_4 emission, which appeared to primarily be coming from a separator.

In order to investigate this attribution further, we analyzed the pre-measurements transects. Because the transects represent individual realizations of the plume, the observed plumes are narrower than the Gaussian model predicts. The Gaussian plume model is meant to predict an average plume profile over ~20 minutes (Fritz et al., 2005). For the narrow transect plumes, the individual plumes can be isolated and quantified. We had only two transects to analyze and there is significant uncertainty of emissions from this approach with few transects (Caulton et al., 2018). Regressing the transect data shows that the plumes have distinct EMRs, with the tank producing a clear ratio ~21% (Figure S2). The separator signal is more variable, but is clearly the source of the ~3% signal (Figure S2). Based on the transect source specific emission estimates, the tank contributed 13% of the total site emissions, in line with the estimate from the parsing method.

References

Caulton, D. R., Li, Q., Bou-Zeid, E., Lu, J., Lane, H. M., Fitts, J. P., et al. (2018). Quantifying uncertainties from mobile-laboratory-derived emissions of well pads using inverse Gaussian methods. *Atmospheric Chemistry and Physics*, *18*(20), 15145–15168. https://doi.org/10.5194/acp-18-15145-2018

Edie, R., Robertson, A. M., Field, R. A., Soltis, J., Snare, D. A., Zimmerle, D., et al. (2020). Constraining the accuracy of flux estimates using OTM 33A. *Atmospheric Measurement Techniques*, *13*(1), 341–353. https://doi.org/10.5194/amt-13-341-2020

Fritz, B. K., Shaw, B. W., & Parnell, C. B. (2005). INFLUENCEOF METEOROLOGICAL TIME FRAMEANDVARIATIONON HORIZONTAL DISPERSION COEFFICIENTSIN GAUSSIAN DISPERSION MODELING. *Transactions of the American Society of Agricultural Engineers*, *48*(3), 1185–1196. https://doi.org//10.13031/2013.18501

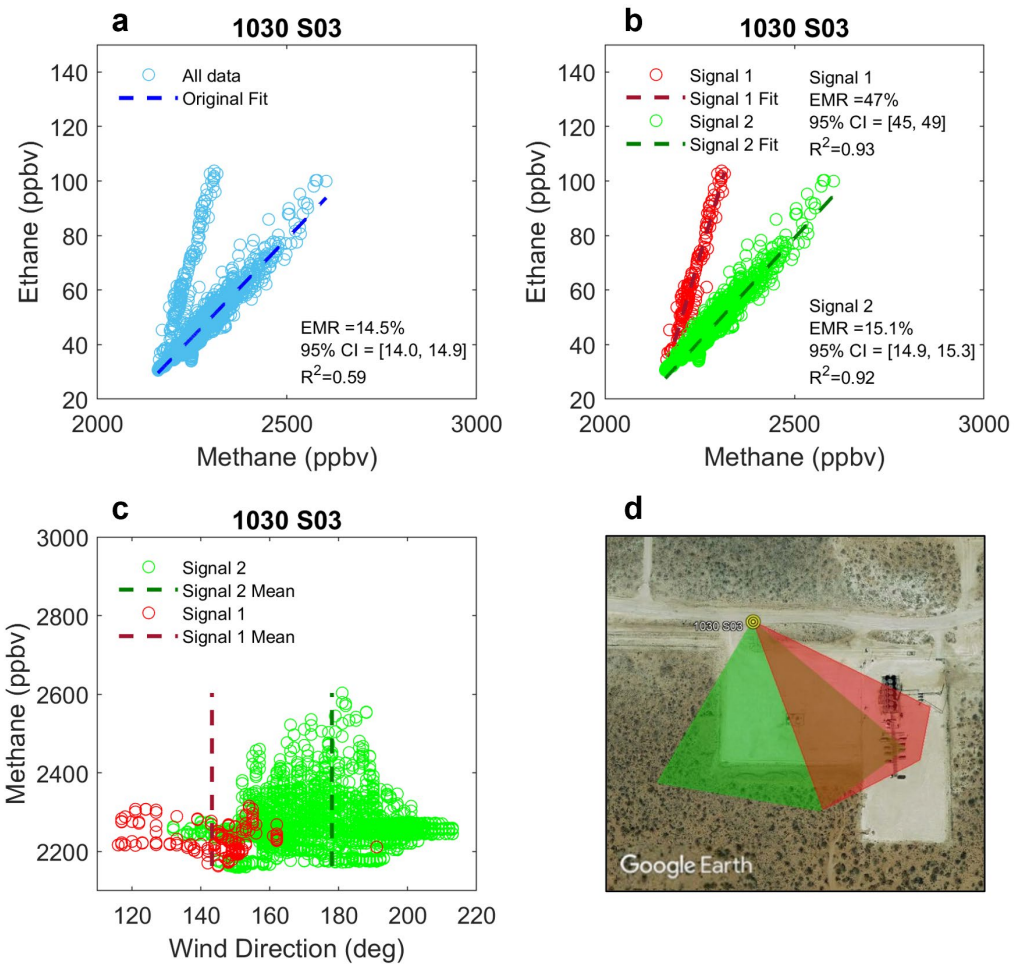

Figure S1. Scatter plot of data for site S03 sampled on 30 Oct. 2020 showing (a) two distinct signals that are not captured by single regression, (b) the signal parsed using PCA, (c) the wind direction data associated with each signal, and (d) the wind direction projected onto site imagery from Google Earth (© Google).

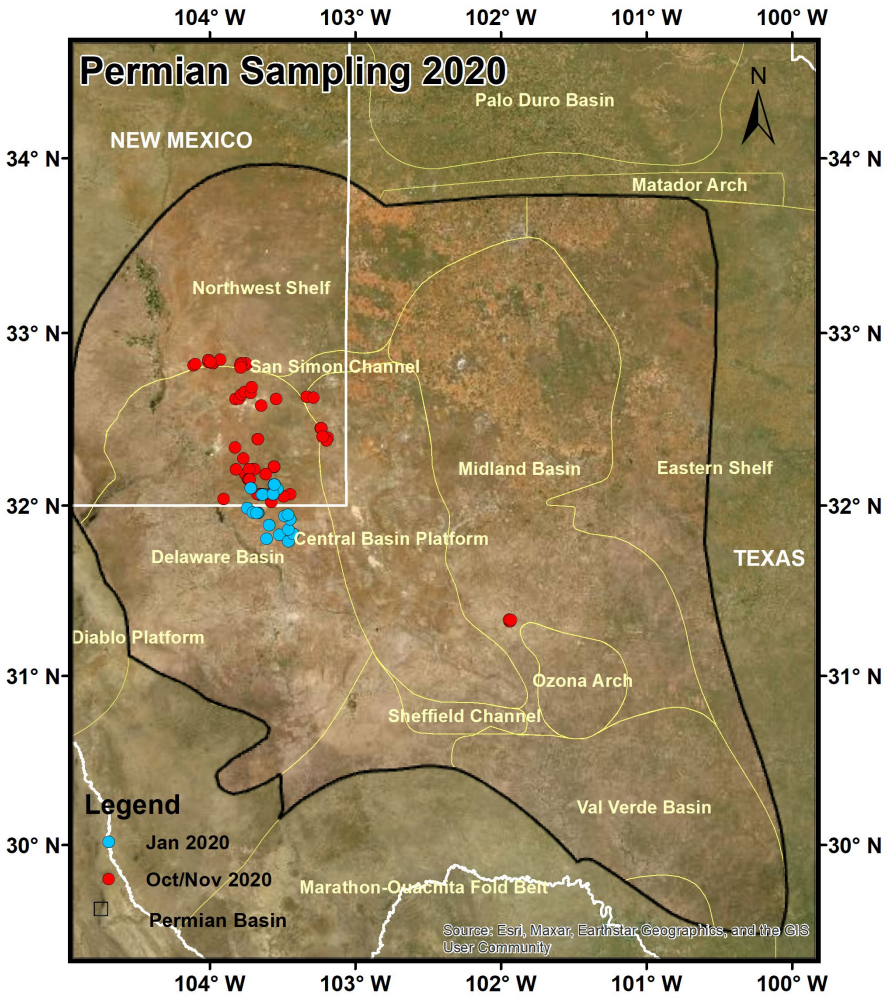

Figure S2. Sampling locations in the Permian Basin in 2020 relative to the entire region. The Permian basin extent is denoted by the thick black line, while individual formations are outlined in yellow. State and international boundary lines are shown in white. The red and blue markers represent the sites sampled. This map was created using ESRI ArcMap 10.8.1 and follows their attribution requirements and terms of use for academic publications, which are available here: https://doc.arcgis.com/en/arcgis-online/reference/static-maps.htm#ESRI_SECTION1_21347CA4FAB14A7E95CE6B738DCA2843

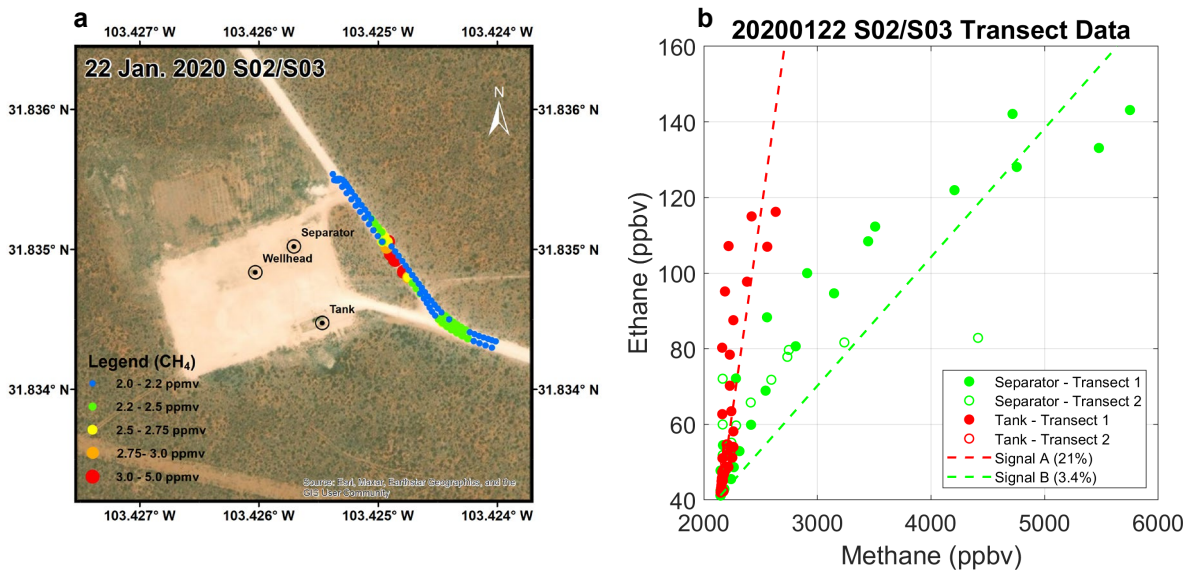

Figure S3. Panel (a) shows an image of sites S02/S03 on 22 Jan. 2020 with the sources on site indicated and the downwind transect colored by CH_4 enhancements. The nominal wind direction was ~245º (SW). This map was created using ESRI ArcMap 10.8.1 and follows their attribution requirements and terms of use for academic publications. Panel (b) shows the regression of the transect data. Plumes have been attributed to the separator and tanks and the ratios from the regression analysis of the OTM have been plotted.

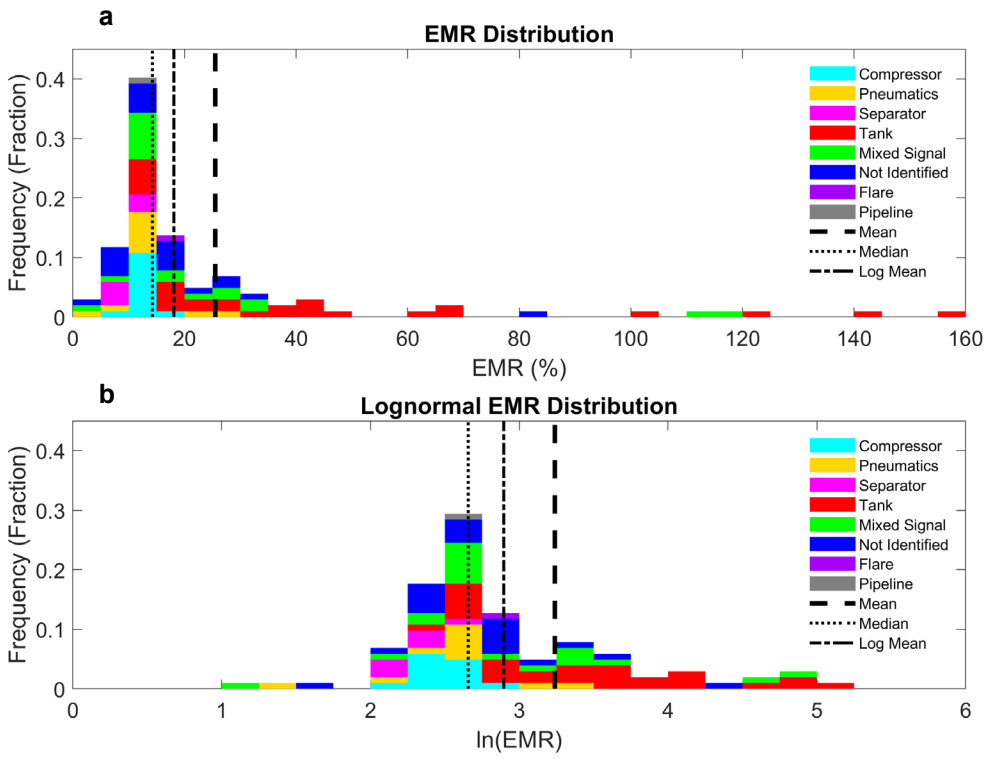

Figure S4. Distribution of EMRs on (a) normal and (b) lognormal axes. Colors represent the contribution to each bin from the specific source type. Also shown are the mean (black dash), median (black dot) and logarithmic mean (black dot/dash) lines.

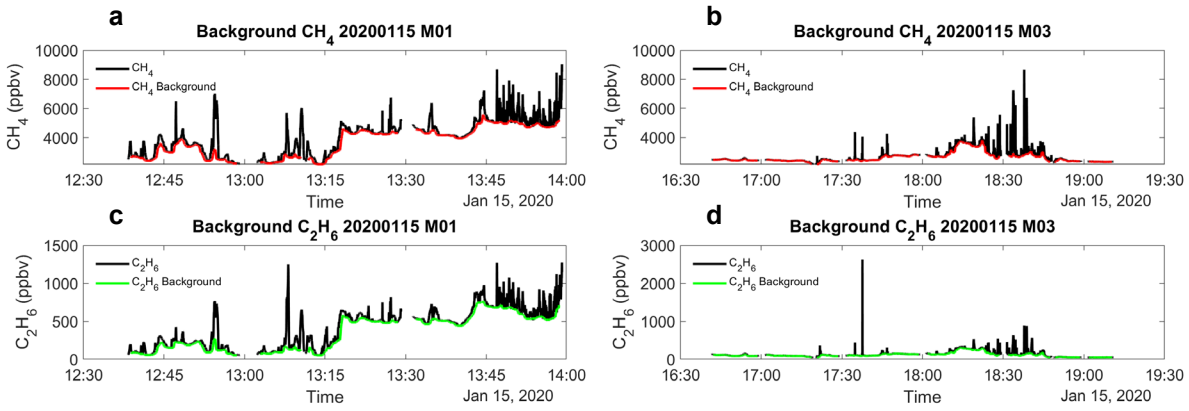

Figure S5. Plots showing the calculated background values for CH_4 (a/b) and C_2H_6 (c/d).

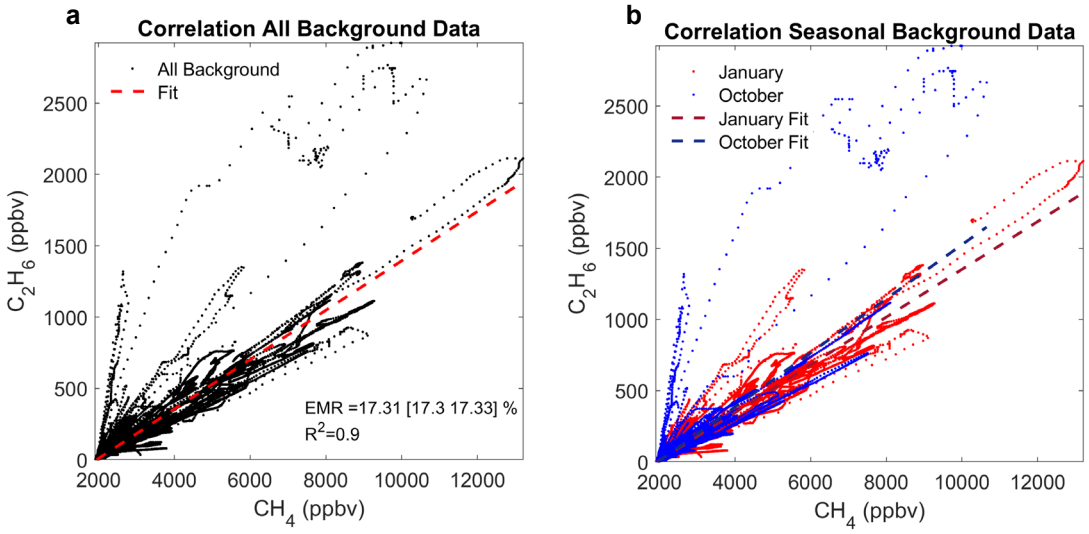

Figure S6. Correlation plots for (a) all background data and (b) background data colored by season collected.

Table S1. Sites with two EMRs and the associated CH_4 and C_2H_6 fluxes for sites where both signals were significant (R^2>0.65).

Site	Signal	EMR (± 95% CI)	R^2	CH_4 Flux (kg hr^{-1})*	C_2H_6 Flux (kg hr^{-1})*	Flux EMR (%)†	Probable Source‡
0115 S01	**Total**	**14.6 (0.3)**	**0.82**	**N/A**	**N/A**	**--**	**Unknown (Tanks, Separator & Compressor present)**
	A	*29.1 (0.8)*	*0.92*	--	--		*CND*
	B	*14.7 (0.1)*	*0.96*	--	--		*CND*
0122 S03	**Total**	**3.32 (0.07)**	**0.82**	**2.02**	**0.18**	**4.7**	**Tank & Pneumatic**
	A	*21 (1)*	*0.9*	*0.14*	*0.06*		*Tank*
	B	*3.48 (0.06)*	*0.9*	*1.88*	*0.12*		*Pneumatic*
1030 S02	**Total**	**11.0 (0.4)**	**0.60**	**1.97**	**0.54**	**14.7**	**Tank & Compressor**
	A	*43 (6)*	*0.71*	*0.25*	*0.20*		*Tank*
	B	*10.6 (0.1)*	*0.94*	*01.72*	*0.34*		*Compressor*
1030 S03	**Total**	**14.5 (0.5)**	**0.59**	**0.58**	**0.15**	**13.2**	**No obvious source (Tanks, Wellhead & Compressor present)**
	A	*47 (2)*	*0.93*	*0*	*0*		*Tanks*
	B	*15.1 (0.2)*	*0.92*	*0.58*	*0.15*		*Compressor/ Wellhead*
1101 S01	**Total**	**10.1 (0.3)**	**0.64**	**N/A**	**N/A**	**--**	**Tank & Separator**
	A	*33 (1)*	*0.86*	--	--		*Tank*
	B	*8.6 (0.1)*	*0.96*	--	--		*Separator*
1103 S04	**Total**	**10.1 (0.2)**	**0.85**	**1.90**	**0.36**	**10.0**	**Tank & Compressor**
	A	*157 (6)*	*0.73*	*0*	*0*		*Tank*
	B	*10.6 (0.1)*	*0.95*	*1.90*	*0.36*		*Compressor*
1105 S06	**Total**	**59 (3)**	**0.43**	**N/A**	**N/A**	**--**	**Tank, Separator, & Intermittent Flare**
	A	*116 (6)*	*0.81*	--	--		*CND*
	B	*15.8 (0.4)*	*0.77*	--	--		*CND*

* Error estimates for OTM 33A derived fluxes are reported to be +54%/-26% (Edie et al., 2020).
† Error estimates for the OTM 33A derived EMRs are calculated to be +76%/-37%.
‡ CND = Could not distinguish. This means that the wind direction did not show sufficient separation and/or sources on site were too close to reasonably distinguish by wind direction analysis.

Table S2. Sites with two EMRs and the associated CH_4 and C_2H_6 Fluxes for sites where only one signal was significant (R^2>0.65).

Site	Signal	EMR (%) (± 95% CI)	R^2	CH_4 Flux (kg hr^{-1})*	C_2H_6 Flux (kg hr^{-1})*	Flux EMR (%)†	Probable Source‡
0116 T02	**Total**	**31.4 (0.8)**	**0.68**	**19.1**	**10.8**	**30.2**	**Unknown**
	A	*33 (4)*	*0.50*	--	--		
	B	*14.3 (0.2)*	*0.90*	--	--		
0117 S01	**Total**	**12.9 (0.3)**	**0.74**	**2.43**	**0.83**	**18.2**	**Compressor (also Separator and Wellhead on site)**
	A	*14.0 (0.2)*	*0.93*	--	--		*CND*
	B	*2.3 (0.3)*	*0.57*	--	--		*CND*
0118 S01	**Total**	**2.2 (0.1)**	**0.35**	**0.28**	**0.03**	**5.5**	**Unknown (Tanks, Combustor and Wellhead on site)**
	A	*25.0 (0.8)*	*0.69*	--	--		*Combustor/ Tanks*
	B	*1.6 (0.3)*	*0.27*	--	--		*Wellhead*
0120 S07	**Total**	**5.9 (0.2)**	**0.64**	**0.39**	**0.07**	**9.6**	**Unknown (Tanks, Compressor, and Wellhead on site)**
	A	*9.7 (0.1)*	*0.91*	--	--		*CND*
	B	*0.8 (0.5)*	*0.41*	--	--		*CND*
1105 S01	**Total**	**3.9 (0.2)**	**0.58**	**0.47**	**0.06**	**6.9**	**Tank (Oil derrick on site)**
	A	*8.7 (0.2)*	*0.87*	--	--		*CND*
	B	*3.6 (0.3)*	*0.60*	--	--		*CND*

*Error estimates for OTM 33A derived fluxes are reported to be +54%/-26% (Edie et al., 2020) and +170%/-50% for transect derived fluxes (Caulton et al., 2018).

† Error estimates for the OTM 33A derived EMRs are calculated to be +76%/-37%.

‡ CND = Could not distinguish. This means that the wind direction did not show sufficient separation and/or sources on site were too close to reasonably distinguish by wind direction analysis.

Table S3. Source categories and the full observations recorded for each site

Source Category	Serial Date	Site	Full Observations
Compressors	20201029	S01	Compressor
	20201030	S03	Compressor
	20201030	S04	Compressor
	20201030	S05	Compressor
	20201030	S06	Compressor
	20201103	S01	Compressor
	20201103	S02	Compressor
	20201103	S03	Compressor
	20201115	S01	Compressor
	20200117	S01	Emissions from compressor stack
	20200120	S01	Emissions from compressor stack
	20200117	T01	Emissions from compressor stack
	20200120	T01	Emissions from compressor stack
Pneumatics	20201031	S02	Emissions from pump wellhead
	20201031	S06	Emissions from pneumatic near pump wellhead
	20200123	S02	Emissions from pneumatic valves on several separators
	20200123	S03	Emissions from pneumatics on separator
	20200123	S04	Emissions from pneumatics on separator
	20200123	S05	Emissions from pneumatics on separators
	20201115	S02	Kimray pneumatic in front of wellhead
	20201115	S05	Pneumatic on separator
	20201108	S02	Pneumatic valve
	20201106	S03	Pneumatic valves near separators
Separators	20201031	S01	Emissions from separator - separator was rusty and had a large nest built on it
	20201105	S03	Separator
	20201105	S04	Separator
	20201105	S05	Separator
	20201110	S02	Separator
	20201110	S06	Separator
Tanks	20200120	S03	Combustor stack on processing tank
	20200118	S02	One of tanks, base of burner
	20201102	S04	Back of tanks - stopped emitting before we could find with FLIR
	20200122	S04	stack on tanks
	20200122	S05	Emissions from stack on tank battery
	20201102	S02	2 tank vent pipes
	20201031	S03	Emissions from tank vent
	20201105	S01	Lower vent hatch on tank
	20201030	S07	Large continuous emissions from tank vent
	20201102	S01	Tank vent
	20201106	S02	Tank vent pipe
	20201107	S05	Tank vent pipe
	20201107	S06	Tank vent pipe
	20201101	S02	Tank vent pipe
	20201025	S01	Vent pipe on tank
	20201106	S01	Tank vent pipes
	20201112	S03	3 tank thief hatches
	20201112	S04	3 tank thief hatches
	20201115	S03	Tank thief hatch
	20201115	S04	Tank thief hatch
	20201105	S02	Tank thief hatch

	20201107	S02	Tank thief hatch
	20201104	S01	Thief hatches on tanks
	20201104	S02	Thief hatches on tanks
	20201107	S01	Thief hatches on tanks
Mixed Signal	20201102	S03	Tank vent pipe and separator
	20201110	S03	Tank thief hatch and pipe going into produced saltwater tan
	20201107	S07	Tank thief hatch and pneumatics near separators
	20201110	S04	Tank thief hatch, pneumatic on separator, and torn pipe going into separator
	20201110	S05	Tank thief hatch, pneumatic on separator, and torn pipe going into separator
	20200120	T03	Leaking from flare, pneumatic valve on separator, and tank vent
	20201105	S06	2 of the separators, vent pipes on 2 of the tanks
	20200109	S01	Leaking everywhere (seps, flare, tanks)
	20200120	S04	Leaking from flare, pneumatic valve on separator, and tank vent
	20200122	S06	Intermittent emissions from flare, emissions from stacks on tanks
	20201112	S02	Flare, thief hatch, tanks
	20200122	S02	Emissions from pneumatic valve on separator and from thief hatch on tanks
	20200122	S03	Emissions from pneumatic valve on separator and from thief hatch on tanks
	20201030	S02	Compressor and tank vent
	20201101	S01	Continuous emissions from tank vent pipe, intermittent emissions from separator
	20201112	S01	3 front tanks, tall back tank, and compressor
	20201103	S04	Compressor and produced saltwater tank
	20201107	S03	Combustor and tank vent pipe
	20201107	S04	Combustor and tank vent pipe
	20201108	S01	Emissions from compressor box near tanks, but flare emitting a lot more
Not Identified	20200123	S01	No obvious source
	20200115	S01	No obvious source
	20200115	S02	No obvious source
	20200120	S02	No obvious source
	20200120	S05	No obvious source
	20200120	S06	No obvious source
	20200120	S07	No obvious source
	20200122	S07	No obvious source
	20201030	S01	No obvious source
	20201031	S05	No obvious source
	20201107	S08	No obvious source
	20201108	S03	No obvious source
	20200120	T04	No obvious source
	20201110	S01	No obvious source
	20201106	S04	No obvious source
	20200118	S01	No obvious source
	20200109	S02	Blank (Aborted)
	20200116	T01	Blank (Transect)
	20200116	T02	Blank (Transect)
	20200116	T03	Blank (Transect)
	20200120	T02	Blank (Transect)

Table S4. EMR and CH_4 Statistics by Source Category

Source	EMR (%)				CH_4 Emission (kg hr^{-1})			n (CH_4)*
	Mean	Weighted Mean	Median	Std. error	Mean	Median	Std. error	
Compressor	12.3	12.4	11.6	0.6	4	2	1	13 (12)
Pneumatics	14	11	13	2	0.7	0.5	0.3	11 (6)
Separator	9.8	9.1	9.5	0.5	0.8	0.5	0.4	7 (5)
Tanks	44	17	27	7	12	1	5	29 (18)
Mixed Signal	27	14	14	7	21	3	17	19 (9)
None	19	16	15	3	2.1	1.8	0.6	21 (11)
Flare	16.3	--	--	--	1.1	--	--	1 (1)
Pipeline Leak	13.7	--	--	--	28	--	--	1 (1)

* n = the number of EMR observations. The number in parentheses is the number of CH_4 emission rate observations.

Table S5. EMR and CH_4 Statistics for Tanks

Tanks	EMR (%)		CH_4 Emission (kg hr^{-1})		Gas Production (Mfc $month^{-1}$)		n (CH_4)*
	Mean	Std. error	Mean	Std. error	Mean	Std. error	
Low EMR	16	1	25	10	4,138	2,016	12 (8)
High EMR	63	10	0.7	0.2	9,040	3,634	17 (12)

* n = the number of EMR observations. The number in parentheses is the number of CH_4 emission rate observations.